university of groningen

University Medical Center Groningen

University of Groningen

The nature of parallax microlensing events towards the Galactic bulge

Smith, M. C.; Belokurov, V.; Evans, N. W.; Mao, S. D.; An, J. H.

Published in:
Monthly Notices of the Royal Astronomical Society

DOI:
10.1111/j.1365-2966.2005.09147.x

IMPORTANT NOTE: You are advised to consult the publisher's version (publisher's PDF) if you wish to cite from it. Please check the document version below.

Document Version
Publisher's PDF, also known as Version of record

Publication date:
2005

Link to publication in University of Groningen/UMCG research database

Citation for published version (APA):
Smith, M. C., Belokurov, V., Evans, N. W., Mao, S. D., & An, J. H. (2005). The nature of parallax microlensing events towards the Galactic bulge. Monthly Notices of the Royal Astronomical Society, 361(1), 128-140. https://doi.org/10.1111/j.1365-2966.2005.09147.x

Copyright
Other than for strictly personal use, it is not permitted to download or to forward/distribute the text or part of it without the consent of the author(s) and/or copyright holder(s), unless the work is under an open content license (like Creative Commons).

Take-down policy
If you believe that this document breaches copyright please contact us providing details, and we will remove access to the work immediately and investigate your claim.

Downloaded from the University of Groningen/UMCG research database (Pure): http://www.rug.nl/research/portal. For technical reasons the number of authors shown on this cover page is limited to 10 maximum.

Download date: 21-05-2019

Mon. Not. R. Astron. Soc. **361,** 128–140 (2005) doi:10.1111/j.1365-2966.2005.09147.x

The nature of parallax microlensing events towards the Galactic bulge

Martin C. Smith,[1,2⋆] Vasily Belokurov,[3⋆] N. Wyn Evans,[3⋆] Shude Mao[2⋆] and Jin H. An[3⋆]

[1] *Kapteyn Institute, PO Box 800, 9700 AV Groningen, the Netherlands*
[2] *Jodrell Bank Observatory, University of Manchester, Macclesfield, Cheshire SK11 9DL*
[3] *Institute of Astronomy, University of Cambridge, Madingley Road, Cambridge CB3 0HA*

Accepted 2005 April 21. Received 2005 April 19; in original form 2004 September 3

ABSTRACT

Perhaps as many as 30 parallax microlensing events are known, thanks to the efforts of the Massive Compact Halo Object (MACHO), Optical Gravitational Lensing Experiment (OGLE), Experience pour la Recherche d'Objets Sombres (EROS) and Microlensing Observations in Astrophysics (MOA) experiments monitoring the bulge. Using Galactic models, we construct mock catalogues of microlensing light curves towards the bulge, allowing for the uneven sampling and observational error bars of the OGLE-II experiment. As a working definition of a parallax event, we require the improvement $\Delta\chi^2$ on incorporating parallax effects in the microlensing light curve to exceed 50. This enables us to carry out a fair comparison between our theoretical predictions and the observations. The fraction of parallax events in the OGLE-II data base is $\sim$1 per cent, though higher fractions are reported by some other surveys. This is in accord with expectations from standard Galactic models. The fraction of parallax events depends strongly on the Einstein crossing time $t_{\rm E}$, being less than 5 per cent at $t_{\rm E} \approx 50$ d but rising to 50 per cent at $t_{\rm E} \gtrsim 1$ yr. We find that the existence of parallax signatures is essentially controlled by the acceleration of the observer normalized to the projected Einstein radius on the observer plane divided by $t_{\rm E}^2$. The properties of the parallax events – time-scales, projected velocities, source and lens locations – in our mock catalogues are analysed. Typically, $\sim$38 per cent of parallax events are caused by a disc star microlensing a bulge source, while $\sim$33 per cent are caused by a disc star microlensing a disc source (of these disc sources, one sixth are at a distance of 5 kpc or less). There is a significant shift in mean time-scale from 32 d for all events to $\sim$130 d for our parallax events. There are corresponding shifts for other parameters, such as the lens-source velocity projected on to the observer plane ($\sim$1110 km s^{-1} for all events versus $\sim$80 km s^{-1} for parallax events) and the lens distance (6.7 kpc versus 3.7 kpc). We also assess the performance of parallax mass estimators and investigate whether our mock catalogue can reproduce events with features similar to a number of conjectured 'black hole' lens candidates.

Key words: gravitational lensing – Galaxy: bulge – Galaxy: centre – Galaxy: kinematics and dynamics.

1 INTRODUCTION

Thousands of microlensing events in the Local Group have been discovered by various collaborations, such as Massive Compact Halo Object (MACHO) (e.g. Alcock et al. 2000), Optical Gravitational Lensing Experiment (OGLE) (e.g. Woźniak et al. 2001; Udalski 2003), Microlensing Observations in Astrophysics (MOA) (e.g. Sumi et al. 2003), Experience pour la Recherche d'Objets Sombres (EROS) (e.g. Afonso et al. 2003) and Pixel Observation on Isaac Newton Telescope - Andromeda Galaxy and Amplified Pixels Experiment (POINT-AGAPE) (e.g. Paulin-Henriksson et al. 2003). The vast majority of these are toward the Galactic centre, many of which were discovered in real-time.[1] The data base of microlensing events provides a unique mass-selected sample with which to probe the mass function of lenses and the mass distribution and dynamics

⋆E-mail: msmith@astro.rug.nl (MCS); vasily@ast.cam.ac.uk (VB); nwe@ast.cam.ac.uk (NWE); smao@jb.man.ac.uk (SM); jin@ast.cam.ac.uk (JHA)

[1] For example, see http://www.astrouw.edu.pl/∼ogle/ogle3/ews/ews.html and http://www.massey.ac./∼iabond/alert/alert.html

© 2005 RAS

Downloaded from https://academic.oup.com/mnras/article-abstract/361/1/128/1021145 by University of Groningen user on 30 November 2018

of the Galaxy (see Paczyński 1996; Evans 2003 for reviews). Unfortunately, the mass of the lens can not be unambiguously determined for most microlensing events because of degeneracies. However, for the so-called exotic microlensing events, which include the finite source size events (Witt & Mao 1994; Gould 1994) and parallax microlensing events (Gould 1992), the degeneracies are partly or wholly broken. Astrometric microlensing offers another exciting possibility whereby to determine the lens mass (e.g. Walker 1995). Astrometric measurements may become feasible with the Very Large Telescope (VLT) interferometer (Delplancke, Górski & Richichi 2001) and future satellite missions such as the *Space Interferometry Mission* (Paczyński 1998) and *GAIA* (Belokurov & Evans 2002).

The standard microlensing light curve follows a characteristic symmetric curve (e.g. Paczyński 1986). However, this is based on the assumption that the relative motions among the observer, lens and source are all uniform and linear. This assumption is clearly wrong in principle as we know the Earth revolves around the Sun, and furthermore, the lens and source may be in binary systems of their own. However, as most microlensing events last of the order of weeks, the effects of acceleration are not noticeable in most events. Nevertheless, for some events, the resulting departures from the standard curve are clearly visible. They can range from a slight asymmetry to dramatic multiple peak behaviour (Smith et al. 2002a). The significance of these so-called parallax events is that they allow an additional constraint to be placed on the lens mass. The parallax events are biased towards (i) more massive, (ii) slow-moving or (iii) closer lenses. The first of these biases means that parallax events offer a powerful way to detect stellar remnants, such as neutron stars and stellar mass black holes (Agol et al. 2003). Combined with other exotic effects, such as finite source size effect, one can derive the lens mass uniquely (e.g. Jiang et al. 2005).

A systematic survey of parallax events of the MACHO data base was performed by Becker (2000). Bennett et al. (2002a) subsequently published the most convincing long-duration events from this survey. Smith, Mao & Woźniak (2002b) have searched systematically for the parallax events in the 3-yr OGLE-II data base. Parallax events have also been found serendipitously in the MOA (Bond et al. 2001) and EROS data bases (Afonso et al. 2003). Table 1 is a compendium of the good and marginal parallax candidates in the direction of the Galactic bulge. The fraction of parallax events in the microlensing data base ranges from around ∼1–10 per cent, although some events are more convincing than others. Additional parallax events have been identified by Popowski et al. (2004), although no model fits were presented for these candidates. Important advances not listed in this table include the detection of the parallax effect in the binary lens events EROS BLG-2000-5 (An et al. 2002) and OGLE-2002-BLG-069 (Kubas et al. 2005), and in the Large Magellanic Cloud single-lens event MACHO LMC-5 (Gould, Bennett & Alves 2004). For all of these events, the parallax effect leads to an accurate determination of the mass of the lens, when combined with the other astrometric or photometric data.

The question naturally arises whether the observed fraction is consistent with theoretical expectations. This is an important question as the number of parallax events depend on the mass function and kinematics of lenses. There have been several previous studies

Table 1. Data for the known parallax events towards the Galactic bulge. Two events (OGLE-1999-BUL-32/MACHO-99-BLG-22 and MACHO-96-BLG-12/EROS-BLG-12) have two separate sets of best-fitting parameters since they have been observed and modelled by two different collaborations. Errors are not given, but can be found in the relevant reference. Values in parentheses indicate the presence of two degenerate parallax fits. Additional MACHO events have been presented in Becker (2000), although the more convincing events from this sample are presented below, since they also appeared in Bennett et al. (2002a,b).

Lightcurve	$t_{\rm E}$ (d)	$\tilde{v}$ (km s^{-1})	$\tilde{r}_{\rm E}$ (au)	Reference
OGLE sc6_2563	71.58	99.3	4.1	Smith et al. (2002a)
OGLE sc20_5748	78.2	53.9	2.4	Smith et al. (2002a)
OGLE sc27_3078	124	23.5	1.7	Smith et al. (2002a)
OGLE sc33_4505	194	56.9	6.4	Smith et al. (2002a)
OGLE sc41_3299	98	41.1	2.3	Smith et al. (2002a)
OGLE sc43_836	45.1	58.0	1.5	Smith et al. (2002a)
OGLE sc26_2218[a,b]	39.53	167	3.8	Smith et al. (2003a)
OGLE-1999-BUL-19	372.0	12.5	2.7	Smith et al. (2002b)
OGLE-1999-BUL-32	640	79	29.1	Mao et al. (2002)
- a.k.a. MACHO-99-BLG-22	560	75	24.3	Bennett et al. (2002b)
OGLE-2000-BUL-43[c]	156.4 (158.2)	40.1 (52.4)	3.6 (4.8)	Soszyński et al. (2001)
OGLE-2003-BLG-238[a]	38.2	652.7	14.4	Jiang et al. (2004)
OGLE-2003-BLG-175[d]	∼63	∼141 (∼106)	∼5.1 (∼3.9)	Ghosh et al. (2004)
MACHO-104-C	110	77	4.9	Bennett et al. (2002a)
MACHO-96-BLG-5	485	30.9	8.7	Bennett et al. (2002a)
MACHO-96-BLG-12	147	47.5	4.0	Bennett et al. (2002a)
- a.k.a. EROS-BLG-12	145.6	43.7	3.7	Afonso et al. (2003)
MACHO-98-BLG-6	245	79	11.2	Bennett et al. (2002a)
MACHO-99-BLG-1	115.5	43.9	2.9	Bennett et al. (2002a)
MACHO-99-BLG-8	120	62	4.3	Bennett et al. (2002a)
EROS-BLG-29	108.3	69.8	4.4	Afonso et al. (2003)
MOA-2000-BLG-11	69.7	42.5	1.7	Bond et al. (2001)
MOA-2003-BLG-37[d]	∼43	∼70 (∼50)	∼1.7 (∼1.3)	Park et al. (2004)

[a]This event also exhibits finite source signatures. [b]The parallax detection becomes marginal if the possibility of small, negative blending is allowed in the fitting. [c]Analysis of additional EROS data for this event has been able to discriminate between the two degenerate sets of parameters, showing that the fit with $t_{\rm E} = 158.2$ d is unfeasible (Le Guillou 2003). [d]Only approximate values are quoted as the parallax parameters have been found to suffer from additional degeneracies.

Downloaded from https://academic.oup.com/mnras/article-abstract/361/1/128/1021145 by University of Groningen user on 30 November 2018

(Buchalter & Kamionkowski 1997; Bennett et al. 2002a). However, these studies have some deficiencies. For example, they all used regular samplings and uniform simulated errors. Even sampling is clearly a gross simplification as there are significant gaps in the observational data, in particular, the annual period (∼late-October – mid-February) during which the bulge cannot be observed. This gap can be especially important for events of sufficiently long duration, since the asymmetric nature of the parallax signal will be more difficult to detect if a significant part of the event lies within this gap.

The purpose of this paper is to conduct a study of parallax events using Monte Carlo simulations for the OGLE-II experiment. We will explicitly account for the uneven sampling, simulate realistic error bars and adopt the same event selection criteria as Woźniak et al. (2001), in order to make a much better comparison between observations and theoretical predictions. The outline of the paper is as follows. We first present the details of our simulations in Section 2. We then make mock catalogues of microlensing events towards the Galactic bulge and compute the fractions of observable parallax events in Section 3. We analyse the properties of the parallax events in our mock catalogues in Section 4. This section includes a number of subsections dealing with event parameters (4.1 – 4.3), mass estimators (4.4) and long duration black-hole candidate events (4.5). We finish with a summary and discussion of strategies for future parallax surveys in Section 5.

2 MONTE CARLO SIMULATIONS

2.1 Parallax microlensing events

The observable quantities for parallax events are the Einstein radius crossing time $t_{\rm E}$ and the projected velocity $\tilde{\boldsymbol{v}}$ on the observer plane. The former quantity is,

$$t_{\rm E} = \frac{r_{\rm E}}{v_\perp}, \qquad r_{\rm E}^2 = \frac{4GM}{c^2} D_{\rm S} x(1-x), \tag{1}$$

where $r_{\rm E}$ is the Einstein radius, M is the mass of the lens, $v_\perp$ is the speed of the lens transverse to the observer-source line of sight, $D_{\rm S}$ is the source distance, $D_{\rm L}$ is the lens distance, while $x = D_{\rm L}/D_{\rm S}$ is the ratio of the distance of the lens to the source. The latter quantity is (Gould 1992),

$$\tilde{\boldsymbol{v}} = \frac{\boldsymbol{v}_\perp}{1-x} = \frac{\boldsymbol{v}_{\rm L} - x\boldsymbol{v}_{\rm S}}{1-x} - \boldsymbol{v}_\odot \tag{2}$$

where $\boldsymbol{v}_{\rm L}$, $\boldsymbol{v}_{\rm S}$ and $\boldsymbol{v}_\odot$ are the velocities of the lens, source and the Sun transverse to the line of sight. The Einstein radius crossing time $t_{\rm E}$ is always measurable for well-sampled microlensing events; however, the projected velocity is only measurable if the magnification fluctuations caused by the motion of the Earth are substantial. The observables $(t_{\rm E}, \tilde{\boldsymbol{v}})$ can be used to construct another useful quantity, namely the Einstein radius projected on the observer plane

$$\tilde{r}_{\rm E} = \tilde{v} t_{\rm E}. \tag{3}$$

2.2 The Galactic model

We assume that the sources and lenses may lie either in the Galactic disc or the bulge. In practice, there may be some contamination from sources in the Sagittarius dwarf galaxy (e.g. Evans 1995; Cseresnjes & Alard 2001). Bennett et al. (2002a) have argued that this may be particularly important for the long-duration events. None the less, the structure of the disrupting Sagittarius dwarf is too irregular and uncertain for reliable modelling and so we do not include it as a source population. In any case, Cseresnjes & Alard argue that the contribution from Sagittarius source events is less than 1 per cent for the OGLE-II fields.

We adopt a value of 8.5 kpc for the Galactocentric distance of the Sun. Using standard cylindrical polars (R, z), the density law of the Galactic disc is (e.g. Binney & Evans 2001)

$$\rho_{\rm L}(R,z) = \rho_0 \exp\left(-\frac{R}{3\ {\rm kpc}}\right) \times \left[0.435\ {\rm sech}^2\left(\frac{z}{220\ {\rm pc}}\right) + 0.565 \exp\left(-\frac{|z|}{440\ {\rm pc}}\right)\right]. \tag{4}$$

This uses the vertical profile found by Zheng et al. (2001) in their studies of disc M dwarfs with the *Hubble Space Telescope*. By counting stars within 5 pc of the Sun (which can be detected through their large proper motions) and using *Hipparcos* parallaxes Jahreiß & Wielen (1997) find that stars contribute 3.9×10^{-2} M$_\odot$ pc^{-3} to the mass density at the plane, which sets the local mass density and hence the overall normalization ρ_0. This is an accurate representation of the local disc, embodying information from local star counts and stellar kinematics. The velocity distribution of disc stars is taken as a Gaussian with a mean $\langle v \rangle = (0, 214, 0)$ km s^{-1} in cylindrical polar coordinates. The disc velocity dispersion is diagonalized along the same cylindrical polar coordinate axes with $\sigma_{RR} = 21$ km s^{-1}, $\sigma_{\phi\phi} = 34$ km s^{-1} and $\sigma_{zz} = 18$ km s^{-1} (Edvardsson et al. 1993).

The density law for the bulge deflectors is

$$\rho_{\rm L}(x', y', z) = \rho_0 \exp\left\{-\left[\left(\frac{x'}{990\ {\rm pc}}\right)^2 + \left(\frac{y'}{385\ {\rm pc}}\right)^2 + \left(\frac{z}{250\ {\rm pc}}\right)^2\right]^{1/2}\right\} \tag{5}$$

with the major axis (x'-axis) in the Galactic plane and oriented at ∼ 24° to the line of sight. This is the E2 model, as suggested by Dwek et al. (1995) and subsequently modified by Stanek et al. (1997). It is a good fit to the near-infrared photometry of the bulge as seen by the *Cosmic Background Explorer (COBE)*. The normalization ρ_0 is set to be 4.46 M$_\odot$ pc^{-3}, which is obtained by setting the total mass within 2.5 kpc of the Galactic centre to be 1.5×10^{10} M$_\odot$. The velocity distribution of the bulge stars is a Gaussian about zero mean. The velocity dispersion tensor is diagonal in the Cartesian coordinates along the axes of the triaxial bulge with $\sigma_{x'x'} = 114$ km s^{-1}, $\sigma_{y'y'} = 86$ km s^{-1} and $\sigma_{zz} = 70$ km s^{-1} (cf. Han & Gould 1995; Evans & Bellokurov 2002).

The mass function $\phi(M)$ – or the number of stars per unit mass – is the multi-part power law taken from equation (4) of Kroupa (2002). This is an initial mass function and so coincides with the present-day mass function below ≈1 M$_\odot$. Above 1 M$_\odot$, the index of the power law is adjusted to give a good representation of the luminosity function in the OGLE-II fields; this gives a steep power law of −7. The luminosity function corresponding to the mass function is computed in the following way. Baraffe et al. (1998) provide mass-to-light coefficients in different bands for stars of different ages with different chemical abundances. We assume a stellar age of 5 Gyr and solar metallicity, then compute the transformation from mass function to luminosity function by numerical differentiation of this data. In our simulations, masses are generated between 0.05 and 5 M$_\odot$. We do not generate masses above 5 M$_\odot$, as the probability distribution is a sharply decreasing function of mass. All the stars with mass below 0.08 M$_\odot$ are treated as dark.

Downloaded from https://academic.oup.com/mnras/article-abstract/361/1/128/1021145 by University of Groningen user on 30 November 2018

2.3 Simulation algorithm

To simulate microlensing events, we must pick the event parameters from the probability distribution

$$P(\ell, b, D_S, m) \propto D_S^2\, \rho_S(\ell, b, D_S)\Psi(m, \ell, b, D_S)\Gamma(\ell, b, D_s) \quad (6)$$

Here, ρ_S is the density of sources, Ψ is the luminosity function and Γ is the microlensing rate at the source location (ℓ, b, D_S). We ascribe the source population to the bulge or disc according to the density at this (ℓ, b, D_S) and choose random velocity components according to the source population. We note that the source velocity probability distributions are separable.

The luminosity function Ψ depends on position because of extinction. The V-band extinction at any location is calculated using the Drimmel & Spergel (2001) extinction law and translated into I-band extinction using $A_v/E(V-I) = 2.1$ (e.g. Popowski 2001). We generate sources within the magnitude range $13.6 < I < 21.0$. The lens mass is generated from

$$P(M) \propto M^{1/2}\phi(M). \quad (7)$$

The flux contributed by the lens is calculated and the microlensing event is retained only if $I < 19$. The cut for objects fainter than $I = 19$ is applied to reduce the problem of blending by faint background sources. Our algorithm therefore only takes the blending by the lens light into account and applies a cut in magnitude to minimize the effects of blending by faint background sources. Although, in practise, the flux from the source can be contaminated by light from other nearby stars, in Section 5 we show that our results are effectively unchanged if we incorporate a simple distribution for this additional blended light.

The differential rate can be written out explicitly as

$$\frac{\mathrm{d}^4\Gamma}{\mathrm{d}^2\boldsymbol{v}_L \mathrm{d}D_L \mathrm{d}M} = \frac{\phi(M)}{\langle M\rangle}\rho_L(\ell, b, D_L)F(\boldsymbol{v}_\perp)2v_\perp r_E(M, D_L) \quad (8)$$

where ρ_L is the total density of lenses, $F(\boldsymbol{v}_\perp)$ is the distribution of relative transverse lens velocities, $\langle M\rangle$ is the average mass while $\boldsymbol{v}_\perp$ is the relative transverse velocity of the lens, as defined in equation (2). So, for the lenses, we choose the distance D_L and velocity $\boldsymbol{v}_L$ from the probability distribution:

$$P(D_L, \boldsymbol{v}_L) \propto \sqrt{D_L(D_S - D_L)}\rho_L(D_L)F(\boldsymbol{v}_\perp)v_\perp \quad (9)$$

The lens population is chosen in this step by comparing the relative densities of disc and bulge lenses at this location. Finally, an impact parameter (defined as the minimum separation between the lens and the Sun–source line of sight, in units of the Einstein radius) is generated in the range $\in [-2, 2]$. This approach to selecting the impact parameter means than a fraction of events will be incorrectly omitted for $\tilde{r}_E \lesssim 1$, since the peak magnification depends on the separation between the lens and the Earth–source line of sight, not the Sun–source line of sight; however, this problem is negligible since only 0.3 per cent of events from our model have $\tilde{r}_E < 1$.

This prescription gives us a microlensing event for our mock catalogue.

2.4 Mock light curves and catalogues

The characteristics of the light curves were chosen to match the 520 event OGLE-II Difference Image Analysis (DIA) microlensing catalogue of Woźniak et al. (2001; see also Woźniak 2000 for a detailed description of the OGLE-II data). These OGLE-II catalogues are constructed from three years of Galactic bulge observations, with observations taken in the I-band once every few nights during the bulge season (typically mid-February until the end of October) resulting in between 200 and 300 observations per light curve. The OGLE-II experiment consists of 49 bulge fields covering a total area of approximately 10 deg^2 (see fig. 1 of Woźniak et al. 2001). Two of the fields are monitored much less frequently and a further three fields had no observations recorded during the first season. The limiting magnitude of the experiment is $I \approx 20$ and the saturation limit is $I \approx 11.5$.

To obtain the time sequence of observations, we randomly select 100 OGLE-II light curves for each field from the variable-star light curves of Woźniak et al. (2002), and then pick one of these time-series at random for each simulated event in the field. We then calculate the flux for each epoch. To do this, we assume that the photometric errors are Gaussian and scale according to the following empirical relation derived from the variable light curves of Woźniak et al. (2002),

$$\sigma_F = 5.04 + 3.58 \times 10^{-3}\, F^{1.04}. \quad (10)$$

Here, the flux (F) and the error on the flux (σ_F) are in units of 10 ADU. These fluxes can be converted into I-band magnitudes through,

$$I(t) = 23.35 - 2.5 \log F(t). \quad (11)$$

As stated in Section 2.3, we simplify our simulations by incorporating the blended flux from the lensed star only, i.e. it is assumed that all of the observed flux comes from either the lensed source or the lens and not from any other nearby stars.

As a final step, we implement the microlensing detection criteria of Woźniak et al. (2001). These criteria were employed to discriminate against variable stars in the OGLE-II Difference Image Analysis (DIA) catalogue and must be applied to our mock catalogues in order to select only events with noticeable brightening and a sufficiently constant baseline.

To assess the credibility of our mock catalogue, we compare it to the observed OGLE-II catalogue of 33 bright events from Sumi et al. (2005). This catalogue of Sumi et al. (2005) is based on events that lie within an extended Red Clump Giant region and are selected to be unblended. We choose this catalogue rather than the 520-event catalogue of Woźniak et al. (2001) as no detailed modelling was carried out on this larger sample. In addition, the catalogue of Woźniak et al. (2001) is affected by blending from unrelated stars near to the source, whereas our mock catalogues only consider blending from the lens. In Fig. 1 we compare two properties, the t_E distribution and the distribution of amplification at the peak. As can be seen from this figure, the two catalogues are in good agreement. For example, the values of the mean t_E are 29.4 d and 28.9 d for the mock catalogue and the observed catalogue, respectively.

3 FREQUENCY OF PARALLAX EVENTS

3.1 Working definition of a parallax event

As a first step in analysing our mock catalogues, we fit all events with both the five-parameter blended Paczyński light curve and seven-parameter blended parallax model. The improvement afforded by the parallax model is recorded as the improvement in χ^2. We also calculate a measure of the signal-to-noise ratio (S/N) for each light curve, defined as the minimum value of F/σ_F for the three points bracketing the maximum amplification.

Before comparing theoretical predictions with observations, we must first investigate what level of improvement in χ^2 is required to classify an event as a parallax event. This is important because

Downloaded from https://academic.oup.com/mnras/article-abstract/361/1/128/1021145 by University of Groningen user on 30 November 2018

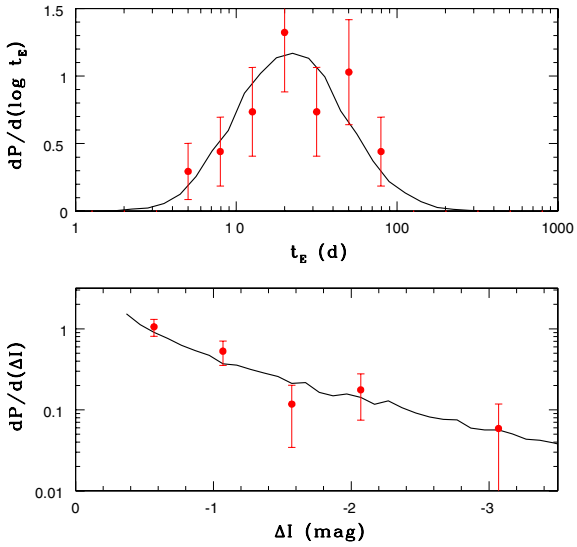

Figure 1. Comparison between our mock catalogue (solid line) and the observed OGLE-II catalogue of 33 bright events (data points) from Sumi et al. (2005), where we have assumed Poisson errors. The top panel shows the time-scale distribution and the lower panel shows the amplitude of the magnification at the peak of the event. To make a fair comparison with the catalogue of Sumi et al. (2005) we have only plotted events from our mock catalogue that are unblended, have magnifications greater than $3/\sqrt{5}$ and have baseline magnitudes brighter than $I = 17$.

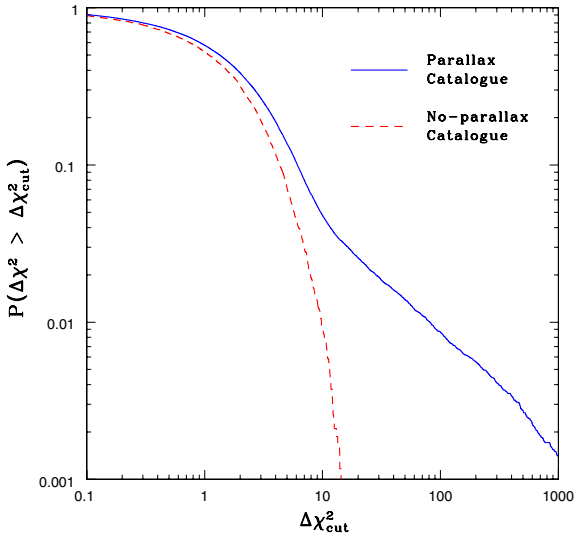

Figure 2. The distribution of $\Delta\chi^2$ for our simulated catalogue (solid) and for the same catalogue but with no parallax signatures (dashed). All events have S/N > 5.

it is conceivable that problems such as scatter in the data could be misidentified as parallax signatures.

To test this, we construct a catalogue of events using our Galactic model but generate light curves with no parallax signatures. We then fit these events with both the standard and parallax models and investigate the distribution of $\Delta\chi^2 = \chi^2_{\rm stan} - \chi^2_{\rm para}$. Fig. 2 shows the distribution of $\Delta\chi^2$ for both the parallax and no-parallax catalogues. The no-parallax distribution shows a rapid decline in the fraction of events with $\Delta\chi^2 > 10$ (less than 1 per cent have $\Delta\chi^2 > 10$). This rapid decline indicates the minimum cut that should be applied in order to identify parallax events. However, when dealing with real data, we must also bear in mind that there may be contamination from other effects, such as binary signatures and/or problems with the data.

Throughout this paper, we adopt three different designations for parallax events: convincing or strong events, with $\Delta\chi^2 > 100$; moderate events, with $\Delta\chi^2 > 50$; and marginal or weak events, with $\Delta\chi^2 > 10$. [If one uses the F-test for the significance of parameters (see Smith et al. 2002b), these limits correspond to $\log p_F < -2$, -10, -20, respectively]. Unless otherwise stated, when we refer to parallax events, the 'moderate' criterion is implied, i.e. $\Delta\chi^2 > 50$. In addition, unless otherwise stated, we restrict ourselves to good quality parallax events with S/N > 5 (as defined at the beginning of this section). In Fig. 3, we show four sample light curves from our mock catalogues. These light curves show clearly how the standard model becomes increasingly less able to fit the mock data as $\Delta\chi^2$ becomes greater. They also illustrate that gaps in the data (in particular, the three month gap between observing seasons) significantly affect our ability to identify parallax events.

The issue of classifying parallax events is further complicated by the fact that even though an event may be displaying parallax signatures, this does not necessarily imply that the parallax parameters can be recovered with a high degree of accuracy due to the degeneracies that are inherent in the parallax formalism (see Gould et al. 2004 and references therein for details of the various types of degeneracies – both continuous and discrete – that can affect parallax events). We illustrate this in Fig. 4 by investigating the distribution of fractional error in recovered projected Einstein radius, i.e. $\delta\tilde{r}_{\rm E} = |(\tilde{r}_{\rm E,fit} - \tilde{r}_{\rm E,true})/\tilde{r}_{\rm E,true}|$. We find that the fraction of events with $\delta\tilde{r}_{\rm E} < 0.3$ is 64, 53 and 23 per cent for our strong, moderate and weak parallax events, respectively. The large fraction of weak parallax events with $\delta\tilde{r}_{\rm E} \approx 1$ are caused by events with $\tilde{r}_{\rm E,fit} \approx 0$. A comprehensive investigation into the nature of the errors for the fitted parameter $\tilde{r}_{\rm E}$ is beyond the scope of this paper.

3.2 Fraction of parallax events

We now analyse the mock catalogue in order to calculate predicted fractions of parallax events. To do this, we compute the total number of events that have $\Delta\chi^2$ greater than a given value. These fractions are plotted in Fig. 5 as a function of the $\Delta\chi^2$ cut for two different choices of S/N cut. This figure shows that for moderate parallax events (i.e. $\Delta\chi^2 > 50$) our catalogues predict a total of ∼1.4 per cent from all events with S/N > 5 or ∼3.6 per cent for S/N > 30. We tabulate our findings in Table 2. For $\Delta\chi^2_{\rm cut} > 10$, the slope of these relationships can be approximated by the following power-laws,

$$P\left(\Delta\chi^2 > \Delta\chi^2_{\rm cut}\right) = 0.22\left(\Delta\chi^2_{\rm cut}\right)^{-0.71} \quad \text{for } \left(\Delta\chi^2_{\rm cut} > 10, \text{S/N} > 5\right) \tag{12}$$

$$P\left(\Delta\chi^2 > \Delta\chi^2_{\rm cut}\right) = 0.44\left(\Delta\chi^2_{\rm cut}\right)^{-0.64} \quad \text{for } \left(\Delta\chi^2_{\rm cut} > 10, \text{S/N} > 30\right). \tag{13}$$

We have also computed the fraction of parallax events on replacing our standard Galactic disc model with a maximal disc model, in which the local disc surface density is increased to $100\,{\rm M}_\odot\,{\rm pc}^{-2}$. The rationale for this is that local disc stars are good candidates as lenses for parallax events, and so the fraction may be a good diagnostic of the local disc density. However, while this change does produce slightly more parallax events, the effect is small and dwarfed by the observational uncertainties.

Downloaded from https://academic.oup.com/mnras/article-abstract/361/1/128/1021145 by University of Groningen user on 30 November 2018

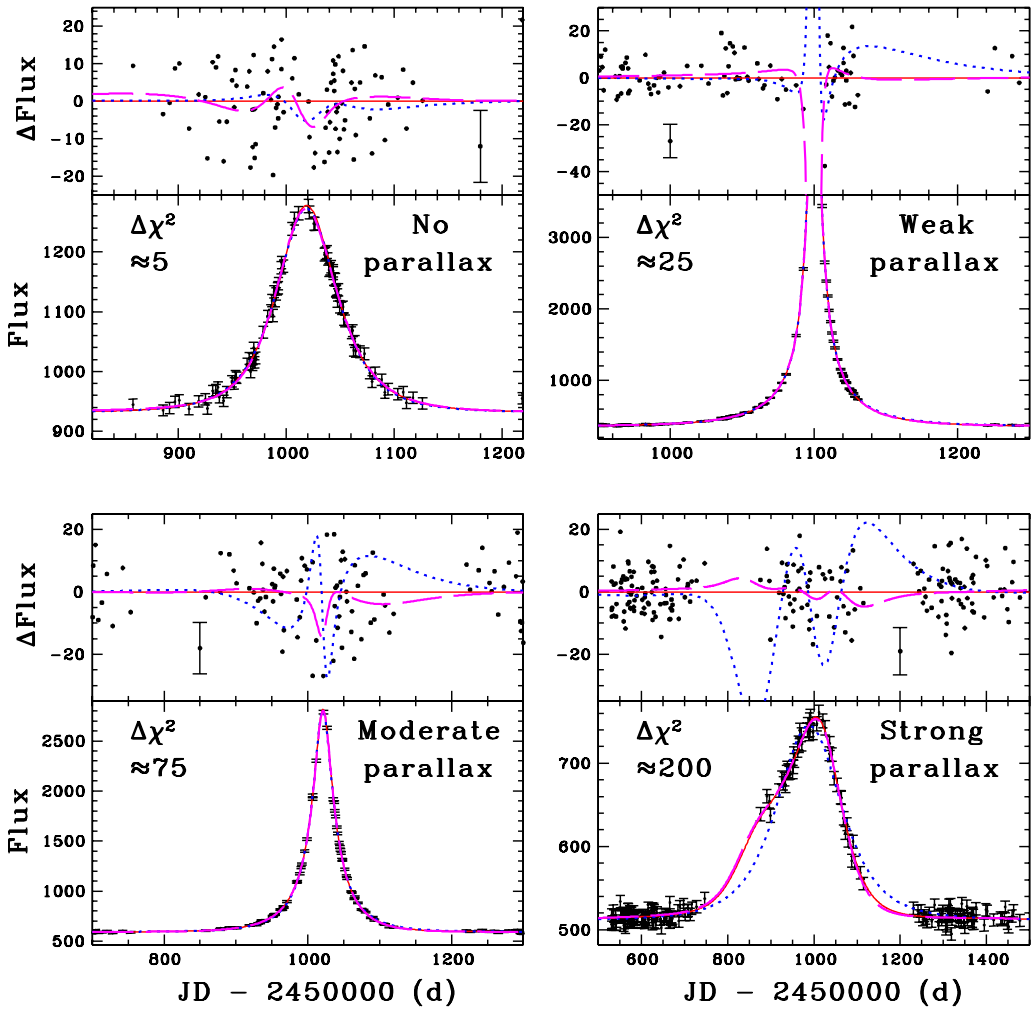

Figure 3. Four sample light curves from our mock catalogues. These light curves illustrate the different cuts that are applied to the catalogue to differentiate between no-, weak-, moderate- and strong-parallax signatures (top left, top right, bottom left and bottom right, respectively). By our definitions, a no-parallax event is one with $\Delta\chi^2 < 10$. The solid line denotes the true light curve, while the dotted and dashed lines correspond to the best-fitting standard and parallax models, respectively. For each light curve we also plot the residuals from the true light curve (top panels). The error bars have been omitted to aid clarity, although a typical error bar has been included – note that this is not an actual data point from the event.

The total fractions from our mock catalogues are in broad agreement with a previous study by Buchalter & Kamionkowski (1997), which estimated that ∼1 per cent of microlensing events towards the bulge should exhibit noticeable parallax signatures. The results from Fig. 5 are also in rough agreement with the fraction of parallax events from different microlensing collaborations, such as MACHO, OGLE and MOA. From a catalogue of 321 events from a 7-yr survey by the MACHO collaboration, ∼2 per cent exhibited convincing parallax signatures and ∼3 per cent exhibited weak parallax signatures (Bennett et al. 2002a). The MOA collaboration found one parallax events (Bond et al. 2001) in their 20-event catalogue from bulge observations in the year 2000, i.e. ∼5 per cent. The fraction of parallax events in the OGLE-II catalogues can be found in two studies: Smith et al. (2002b) found one convincing parallax event from a sample of 512 events, although a number of parallax events were subsequently found to have been omitted from this 512 event sample (e.g. Mao et al. 2002; Smith et al. 2002a); and Sumi et al. (2005) found one parallax event[2] in their sample of ∼30 bright red clump giant sources. Although the above results seem to be consistent, a recent study by the EROS collaboration (Afonso et al. 2003) reported a much higher fraction of parallax events; from a total of 16 red clump giant events they identified 2 convincing parallax events, i.e. 12.5 per cent. We return to the issue of these EROS parallax events in the Discussion, below, but the level of discrepancy (or agreement) between these fractions must be taken with caution as all are subject to small number statistics. In addition, such comparisons are affected by the different properties of the catalogues, i.e. the observing strategy and duration of each project, etc. When comparing such fractions, we should also bear in mind the fact that our mock catalogues are restricted to events with *I*-band baseline magnitudes brighter than 19 mag.

4 THE PROPERTIES OF THE PARALLAX EVENTS

In this Section, we investigate various properties of parallax events in our mock catalogue in order to understand their nature. We utilize the criteria defined in Section 3.1 to refer to strong, moderate and weak parallax events and enforce a minimum signal-to-noise ratio

[2] This parallax event is the same as the one discovered in Smith et al. (2002b).

Downloaded from https://academic.oup.com/mnras/article-abstract/361/1/128/1021145 by University of Groningen user on 30 November 2018

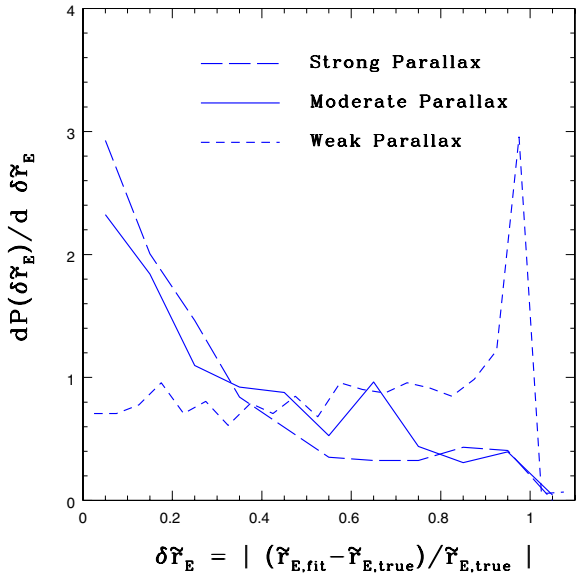

Figure 4. The distribution of fractional error in the recovered projected Einstein radius, i.e. $\delta\tilde{r}_{\rm E} = |(\tilde{r}_{\rm E,fit} - \tilde{r}_{\rm E,true})/\tilde{r}_{\rm E,true}|$. This is shown for our three levels of parallax events, strong (long dash), moderate (solid line) and weak (short dash). The large fraction of weak parallax events with $\delta\tilde{r}_{\rm E} \approx 1$ are caused by events with $\tilde{r}_{\rm E,fit} \approx 0$.

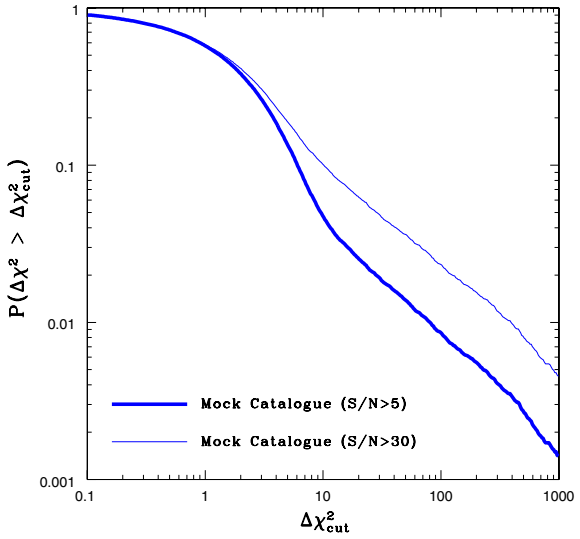

Figure 5. The cumulative fraction of parallax events in the mock catalogue, i.e. the fraction of parallax events for different cuts of $\Delta\chi^2$. The thick and thin lines are for events with S/N > 5 and S/N > 30 respectively.

Table 2. The percentage of parallax events using the criteria defined in Section 3.1 as a function of S/N cut.

S/N cut	Percentage of parallax events		
	Weak parallax ($\Delta\chi^2 > 10$)	Moderate parallax ($\Delta\chi^2 > 50$)	Strong parallax ($\Delta\chi^2 > 100$)
5	4.6	1.4	0.8
15	7.1	2.3	1.5
30	10.0	3.6	2.3

(S/N) of 5. We deal with the event time-scales, lens and source distances, and projected velocities in turn. Table 3 summarizes the mean and median values for these quantities. We also assess the performance of parallax mass estimators and investigate whether our mock catalogue can reproduce events with features similar to a number of conjectured 'black hole' candidates.

4.1 Event time-scale

Fig. 6 shows the distribution of the true event time-scale[3] (i.e. not the fitted time-scale). As expected, the parallax events all lie in the long duration tail of the time-scale distribution. While the $t_{\rm E}$ distribution for all events in our mock catalogue peaks around $t_{\rm E} \approx 20$ d, parallax events peak around $t_{\rm E} \approx 100$ d. Although we might expect parallax events to be detected at very large time-scales, few are seen with $t_{\rm E} \gtrsim 500$ d. This is because our simulated light curves are based on the 3-yr data set from OGLE-II. The microlensing event detection drops off sharply for $t_{\rm E} \gtrsim 500$ d, as such long events do not pass the constant baseline criterion necessary to differentiate microlensing events from variable stars (Woźniak et al. 2001).

Given the quality and sampling of the OGLE-II data, it is unlikely that we can detect parallax signatures for events with $t_{\rm E} \lesssim 50$ d, even for weak parallax events. The upper panel of Fig. 6 shows that at $t_{\rm E} \approx 50$ d, the fraction of events that display parallax signatures is less than ∼5 per cent (0.7, 1.5, and 7.2 per cent for strong, moderate and weak parallax events). The prospect of obtaining or constraining the parallax parameters for such short-duration events can be helped by more frequent sampling and/or improved photometric accuracy, such as that afforded by the numerous microlensing follow-up networks (e.g. Jiang et al. 2005); however, it is known that such short-duration events are affected by significant degeneracies (e.g. Gould 1998).

The fraction of events that display moderate parallax signatures exceeds 50 per cent for events with $t_{\rm E} \gtrsim 1$ yr. However, the fact that the fraction of parallax events only reaches ∼50 per cent for $t_{\rm E} \approx 1$ yr shows that even for such long-duration events, the presence of strong parallax signatures is not guaranteed.

4.2 Lens and source distances

Fig. 7 shows the distributions of lens and source distances. The lensed sources are preferentially on the far side of the Galactic centre (see also Table 3, which shows that the mean source distance for all events is 9.7 kpc), as these sources have more foreground lensing stars, i.e. the optical depth is greater for sources behind the Galactic centre. They will appear fainter (Stanek 1995) and may have different proper motions from the overall population of stars (Mao & Paczyński 2002).

From Fig. 7, it can be seen that nearby lenses are favoured for parallax events. This is due to the fact that nearby lenses have smaller values of $\tilde{v}$ and $\tilde{r}_{\rm E}$ owing to the smaller projection factor (see Section 4.3).

It has been suggested (e.g. Smith et al. 2002b) that parallax events may be preferentially caused by so-called disc–disc lensing, which

[3] It should be noted that the underlying distribution of time-scale is mainly controlled by the choice of mass function (see, for example, the left-hand panel of fig. 10 in Alcock et al. 2000); however, the purpose of our work is to investigate parallax events and so we do not concern ourselves with undertaking a detailed analysis of the overall form of the time-scale distribution.

Downloaded from https://academic.oup.com/mnras/article-abstract/361/1/128/1021145 by University of Groningen user on 30 November 2018

Table 3. Mean (median) values for the microlensing parameters discussed in Section 4.

	Mean (median) values			
	All events	Weak parallax	Moderate parallax	Strong parallax
$t_{\rm E}$ (d)	32.1 (22.9)	91.2 (73.4)	130.4 (105.8)	141.6 (112.0)
$\tilde{r}_{\rm E}$ (au)	10.3 (8.3)	6.4 (5.2)	4.8 (3.9)	4.5 (3.8)
$\tilde{v}$ (km s^{-1})	1108.6 (609.0)	247.2 (113.9)	80.1 (61.4)	69.6 (52.8)
$D_{\rm S}$ (kpc)	9.7 (9.2)	9.6 (9.0)	9.2 (8.6)	9.1 (8.6)
$D_{\rm L}$ (kpc)	6.7 (7.0)	4.7 (4.4)	3.7 (3.1)	3.5 (2.9)

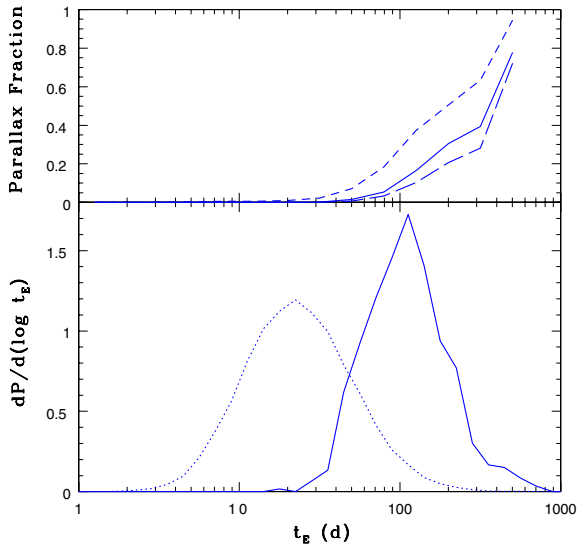

Figure 6. The lower panel shows the distribution of event time-scales for all events (dotted line) and parallax events (solid line) in our mock catalogue. The upper panel shows the corresponding fraction of parallax events as a function of time-scale for strong, moderate and weak parallax events (long dash, solid and short dash, respectively). Note that these plots use the true event time-scale, not the fitted event time-scale.

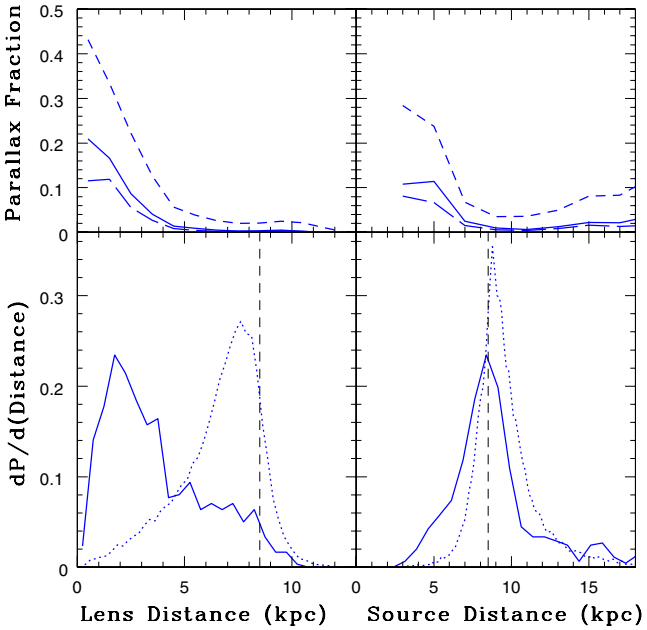

Figure 7. The upper panels show the fraction of events that are classified as parallax as a function of lens–source distance for strong, moderate and weak parallax events (long dash, solid and short dash, respectively). The lower panels show the distributions of lens and source distances for all events (dotted line) and parallax events (solid line) in our mock catalogue. The vertical dashed lines at 8.5 kpc denote the centre of the Galaxy in our simulations.

refers to events in which both the source and lens lie in the disc. For such events the lens, source and observer are all co-rotating with the Galactic disc, producing small relative transverse velocities and hence enhancing the probability of detecting parallax signatures. This phenomenon can be seen in the right-hand panel of Fig. 7, which exhibits a peak in the fraction of parallax events for nearby sources. However, the ratio of parallax events with disc sources is reduced due to the fact that the overall density of sources in the near side of the disc is only small. For our Galactic model we predict that ∼5 per cent of parallax events have lensed sources lying within 5 kpc, which is a significant fraction when one considers that only 0.5 per cent of all microlensing events have sources located in this region.

In Table 4, we compare the relative abundance of parallax events within the different lens–source configurations, such as for disc–bulge events (i.e. events in which the lens is in the disc and the source is in the bulge), etc. Clearly, one can see that the majority of parallax events are due to the disc–disc and disc–bulge events, namely ∼33 and ∼38 per cent respectively. This can be contrasted with the most common configuration for all microlensing events, which is bulge–bulge. Note that our parallax events have ∼5 per cent of sources within 5 kpc, which is slightly larger than the estimate of less than 3 per cent that was predicted by the simulations of Bennett et al. (2002a).

4.3 Projected Einstein radius and projected lens velocity

Fig. 8 plots the distribution of the Einstein radius projected into the observer plane $\tilde{r}_{\rm E}$ and the projected velocity $\tilde{v}$ for all events and for parallax events. This shows that parallax signatures are more readily detectable for events with small values of $\tilde{r}_{\rm E}$ and $\tilde{v}$, as predicted by Smith et al. (2002a). This can be understood, on considering that the projected velocity of the lens should be comparable to (and preferably less than) the orbital velocity of the Earth, which is $v_\oplus \sim$ 30 km s^{-1}. The reason why smaller values of $\tilde{r}_{\rm E}$ are favoured is because this parameter determines the length scale on which the magnification is calculated. This means that the magnitude of the deviations is determined by the magnitude of the Earth's motion relative to this projected Einstein radius, i.e. in general, the larger the projected Einstein radius, the smaller the deviations.

In Fig. 9, we show the joint distribution of $t_{\rm E}$ and $\tilde{v}$, which – as expected – shows that parallax events preferentially have large $t_{\rm E}$ and small $\tilde{v}$. From this figure, it is clear that the ability to detect parallax signatures is controlled by the quantity $\tilde{v}/t_{\rm E} = \tilde{r}_{\rm E}/t_{\rm E}^2$. For a given acceleration a, the dimensionless parameter $\mathcal{A} = a/(\tilde{r}_{\rm E}/t_{\rm E}^2)$

Downloaded from https://academic.oup.com/mnras/article-abstract/361/1/128/1021145 by University of Groningen user on 30 November 2018

Table 4. The percentage of events as a function of lens–source configuration for all events and weak-, moderate- and strong-parallax events. For the values without parentheses, a disc star is defined as one drawn from the population described by equation (4), while a bulge star is drawn from equation (5). Bennett et al. (2002a) used a different nomenclature, defining all stars within 3.5 kpc of the Galactic centre as 'bulge' and all stars outside 3.5 kpc of the Galactic centre as 'disc'. To enable comparison with Bennett et al.'s results, we give in parentheses the values corresponding to these definitions. Note that the disc–disc events are subdivided according to whether the disc stars reside on the near or far side of the Galactic centre.

Lens	Source	Percentage of events with given lens-source configuration			
		All events	Weak parallax	Moderate parallax	Strong parallax
near disc	near disc	3.1 (0.5)	19.4 (3.1)	33.2 (5.2)	36.3 (5.7)
near disc	far disc	12.0 (0.9)	9.4 (3.4)	7.5 (4.7)	8.9 (5.1)
far disc	far disc	1.5 (0.1)	0.9 (0.0)	0.5 (0.0)	0.8 (0.0)
disc	bulge	29.6 (17.1)	39.6 (49.7)	38.4 (62.8)	36.9 (65.9)
bulge	bulge	34.0 (71.6)	14.3 (31.3)	8.9 (17.4)	7.3 (13.3)
bulge	disc	19.9 (9.8)	16.3 (12.4)	11.6 (9.9)	9.8 (10.0)

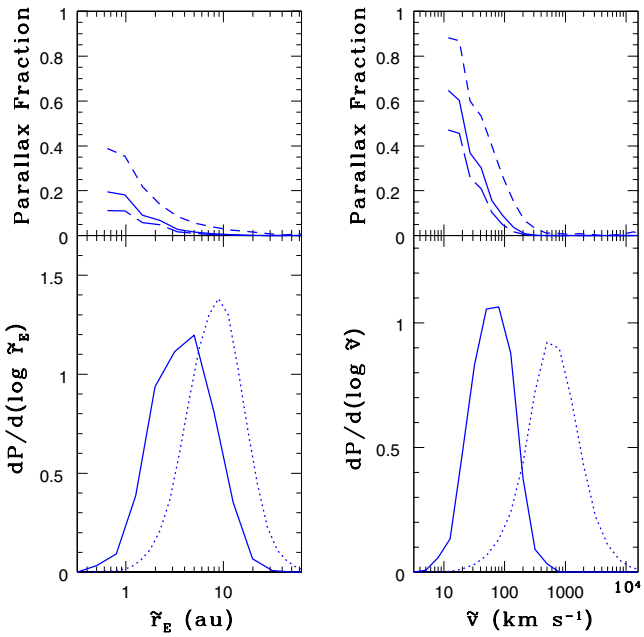

Figure 8. The lower panels show the distribution of the Einstein radius projected into the observer plane ($\tilde{r}_{\rm E}$; left) and the projected lens velocity on the observer plane ($\tilde{v}$; right) for all events (dotted line) and parallax events (solid line). The upper panels show the fraction of events that display parallax signatures as a function of $\tilde{r}_{\rm E}$ (left) and $\tilde{v}$ (right) for strong, moderate and weak parallax events (long dash, solid, and short dash, respectively). Note that these plots use the true values for $\tilde{r}_{\rm E}$ and $\tilde{v}$, not the fitted values.

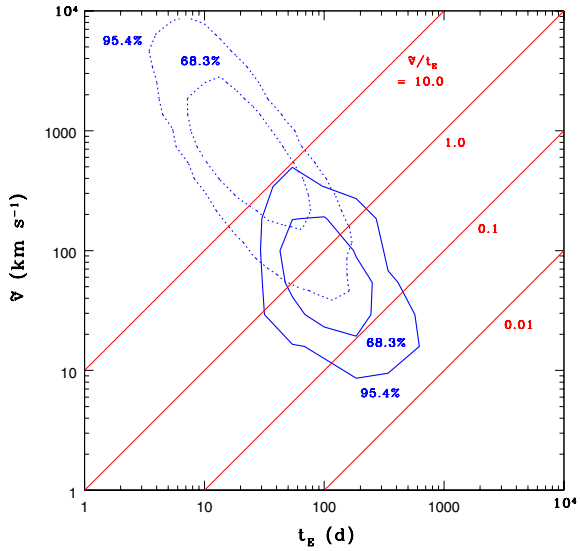

Figure 9. Contour plot showing the joint distribution of event time-scale and projected lens velocity on the observer plane for all events (dotted) and parallax events (solid). The four diagonal lines indicate constant $\tilde{v}/t_{\rm E} = \tilde{r}_{\rm E}/t_{\rm E}^2 = 10.0, 1, 0.1, 0.01\,{\rm km\,s^{-1}\,d^{-1}}$. If we approximate the Earth's projected acceleration to be $a \approx 0.3$ km s^{-1} d^{-1} (i.e. averaged over the whole year), then these contours correspond to $\mathcal{A} = a/(\tilde{v}/t_{\rm E}) \approx 0.03, 0.3, 3, 30$. This dimensionless acceleration parameter $\mathcal{A}$ effectively controls the significance of the parallax deviations (see Section 4.3).

describes the deviation of the trajectory from a straight line (Smith, Mao & Paczyński 2003b). Parallax deviations are caused by the Earth's orbital acceleration. Although the magnitude of this acceleration is constant in the ecliptic plane, when projected into the lens plane it is no longer constant and so a varies throughout the year. However, most parallax events last for a sufficiently long duration for the average value of a to be used. This means that the quantity $\tilde{r}_{\rm E}/t_{\rm E}^2$ effectively determines the value of $\mathcal{A}$ and hence controls the significance of the deviation arising from the Earth's motion, i.e. a larger $\tilde{r}_{\rm E}/t_{\rm E}^2$, indicates that the parallax effect will be more difficult to detect and vice versa. We return to the issue of the $\tilde{r}_{\rm E}$ distribution in the discussion, where we compare our predictions to the observed distribution.

For a parallax event, it is possible to determine the orientation of $\tilde{\mathbf{v}}$, from which we can gain additional information regarding the event. In Fig. 10, we show the distribution of this angle transformed into Galactic coordinates (θ_G), where θ_G is measured from the Galactic plane (in the direction of rotation) towards the North Galactic pole. From this figure, it can be seen that parallax events preferentially have $\tilde{\mathbf{v}}$ orientated in a direction parallel to the ecliptic plane. This can be understood when one considers that trajectories perpendicular to the ecliptic plane will have less time to be affected by the Earth's motion, compared to trajectories that pass parallel to the ecliptic plane, i.e. for perpendicular trajectories the Earth's acceleration will only affect the peak of the light curve (Bennett et al. 2002a). The orientation of $\tilde{\mathbf{v}}$ is also affected by the fact that parallax events are commonly the result of bulge sources being lensed by foreground disc stars (see Section 4.2). For the disc–bulge configuration, $\tilde{v}$ is,

Downloaded from https://academic.oup.com/mnras/article-abstract/361/1/128/1021145 by University of Groningen user on 30 November 2018

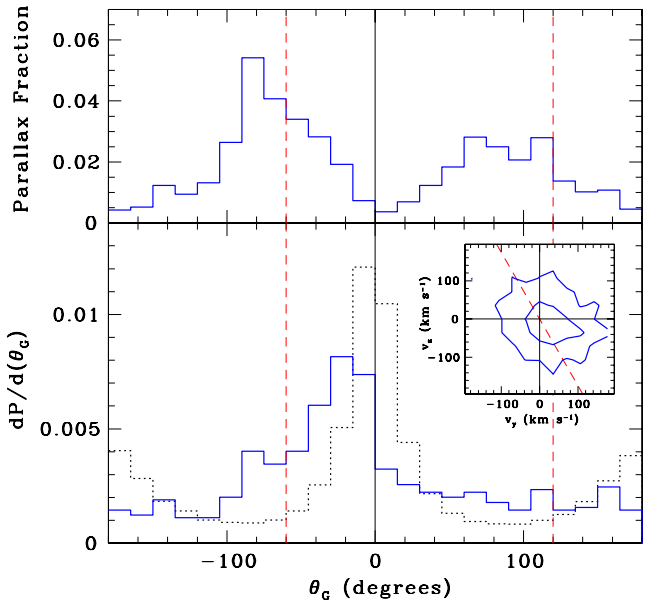

Figure 10. The lower panel shows the distribution of the projected velocity angle, θ_G, for all events (dotted line) and moderate parallax events (solid line) in our mock catalogue. θ_G is measured in Galactic coordinates from the Galactic plane (in the direction of rotation) towards the North Galactic pole. The inset shows the projected velocity distribution in Galactic coordinates, where the horizontal axis corresponds to the direction of rotation and the vertical axis corresponds to the North Galactic Pole. The contours correspond to the 68.3 and 95.4 per cent confidence intervals. The upper panels show the fraction of events that are classified as moderate parallax events as a function of the projected velocity angle. The dashed lines denote the orientation of the ecliptic plane in this coordinate system.

on average, orientated along the direction of rotation of the Galactic plane owing to the fact that the Sun and the lenses share a common motion in the plane of the disc. This enhances the fraction of parallax events with $-90^\circ < \theta_G < 90^\circ$, as can be seen from Fig. 10.

We also investigated the radial velocities of the source stars for our mock catalogues. No significant difference was found between the parallax events and all lensed sources.

4.4 Mass estimators

Bennett et al. (2002a) and Agol et al. (2002) proposed very similar techniques for estimating the mass of the lens for parallax events. Using our mock catalogues, we can assess the reliability of their estimator.

Agol et al. (2002) assume that the source and lens populations are both characterized by Gaussian velocity distributions with means $\langle \boldsymbol{v_L} \rangle$ and $\langle \boldsymbol{v_S} \rangle$ and dispersions $\boldsymbol{\sigma_L}$ and $\boldsymbol{\sigma_S}$, diagonalized in Galactic longitude and latitude (ℓ, b). Specializing to the case of a power-law mass function $n(m) \propto m^{-\beta}$, Agol et al.'s (2002) maximum likelihood estimator becomes:

$$L(x|\tilde{\boldsymbol{v}}, t_{\rm E}) \propto x^{\beta-1}(1-x)^{5-\beta}\frac{\rho_{\rm L}(x)}{\sigma_\ell \sigma_b} \times \exp\left[-\left(\frac{v_\ell^2}{2\sigma_{L,\ell}^2}+\frac{v_b^2}{2\sigma_{L,b}^2}\right)\right], \quad (14)$$

where

$$(v_\ell, v_b) = \langle \boldsymbol{v_L} \rangle - x\langle \boldsymbol{v_S} \rangle - (1-x)(\boldsymbol{v}_\odot + \tilde{\boldsymbol{v}}), \quad (15)$$

and

$$\sigma_\ell^2 = \sigma_{L,\ell}^2 + x^2\sigma_{S,\ell}^2, \qquad \sigma_b^2 = \sigma_{L,b}^2 + x^2\sigma_{S,b}^2. \quad (16)$$

$L(x|\tilde{\boldsymbol{v}}, t_{\rm E})$ gives the likelihood of a lens lying at a fractional distance $x = D_{\rm L}/D_{\rm S}$, given the observables $\tilde{\boldsymbol{v}}$ and $t_{\rm E}$. This is obtained using Bayes' theorem, assuming uniform priors in lens distance and no errors on the velocity and time-scale measurements. It can be converted to a likelihood in mass m using

$$m(x) = \frac{\tilde{v}^2 t_{\rm E}^2 c^2 (1-x)}{4GxD_{\rm S}}. \quad (17)$$

As the mass functions in our simulations are more complicated than simple power laws, we explore two different choices, namely $\beta = 0$ and $\beta = 1.5$. In the latter case, equation (14) reduces to a formula proposed by Bennett et al. (2002a).

The estimator also assumes that the distance of the source $D_{\rm S}$ is known and that the lensing population is identifiable, so that an informed choice for the density $\rho_{\rm L}$ can be made. We extracted 728 events from our mock catalogue that pass Woźniak et al.'s (2001) criteria. These are moderate parallax events with $\Delta\chi^2 > 50$ and S/N > 5. We use the fitted values of $\tilde{\boldsymbol{v}}$, $t_{\rm E}$, together with the known source distance $D_{\rm S}$ and the known type of deflector population to compute the estimated mass. Of course, the accuracy in the estimate can be calculated, as the true mass is known.

Fig. 11 shows histograms of the logarithm of the ratio of the recovered mass to the true mass for the 89 events caused by bulge deflectors (left panels) and 639 events caused by disc deflectors (right panels) using the likelihood estimator with $\beta = 1.5$ and $\beta = 0$. For the bulge lenses, both estimators give a similar performance with mean percentage errors of -22 per cent ($\beta = 0$) and -45 per cent ($\beta = 1.5$). A negative value of the mean percentage error implies that the estimators typically underestimate the mass. For the disc lenses, the estimators tend to overestimate the mass,

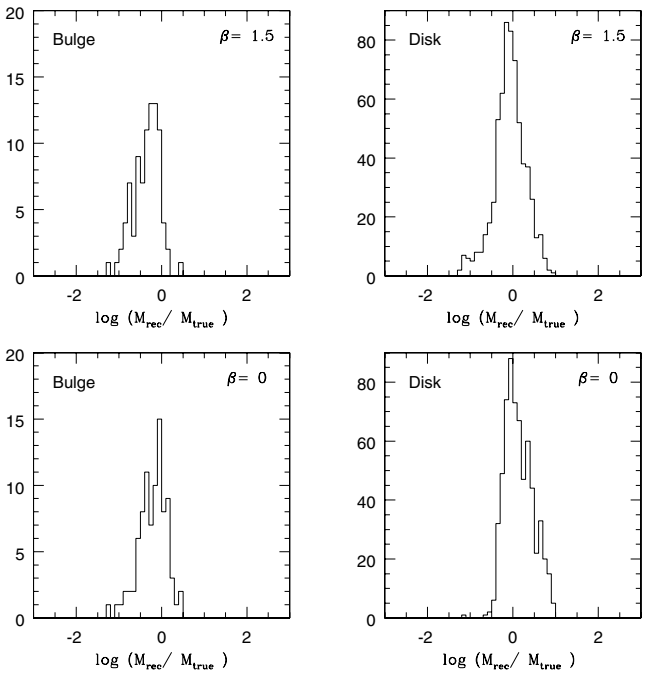

Figure 11. The error distributions of the estimators of the mass of the lens of a parallax event using $\beta = 1.5$ (above) and $\beta = 0$ (below) in equation (14). The results for bulge deflectors are shown on the left, those for disc deflectors on the right. The abscissa is the logarithm of the ratio of the recovered to the true mass.

Downloaded from https://academic.oup.com/mnras/article-abstract/361/1/128/1021145 by University of Groningen user on 30 November 2018

with a mean percentage error of 85 per cent for $\beta = 0$ compared to 20 per cent for $\beta = 1.5$. The simulations use more complicated mass functions than power laws. It is noteworthy that the effect of using a simple power-law mass function in the likelihood estimator (which is needed to perform the integrals) is to cause systematic offsets in the recovered masses as compared to the true masses.

The interpretation of the effectiveness of these mass estimators suffers from an additional complication. As was shown in Section 3.1, the accurate recovery of the parallax parameters such as $\tilde{\mathbf{v}}$ is not guaranteed, even for our convincing parallax events (see Fig. 4). Clearly these mass estimators cannot be expected to perform reliably if the parallax parameters have not been determined accurately from the observed light curves.

4.5 Long duration events and black hole candidate lenses

Our simulations can also be used to investigate the nature of observed long-duration microlensing events, a number of which have been speculated to have been caused by black hole lenses.

In our model, we do not include any stellar remnant populations. However, white dwarfs ($M \sim 0.6$ M$_\odot$), neutron stars ($M \sim 1.4$ M$_\odot$) and black holes ($M \sim$ several M$_\odot$) must exist in the Galactic disc, and so their contribution to parallax events is not accounted for in our model. For long durations ($t_{\rm E} \gtrsim 100$ d), the time-scale distribution asymptotically approaches a power law (Mao & Paczyński 1996). As a result, the fraction of events contributed by stellar remnants reaches an asymptotic value, determined entirely by the mass function. The relative fraction is weighted according to $\sim M^2 n(M)\,{\rm d}M$, and hence favours massive lenses (Agol et al. 2002). If we adopt a mass function for stellar remnants (e.g. Gould 2000; Han & Gould 2003), we find that the fraction of long-duration events contributed by stellar remnants is about 56 per cent. Therefore our predicted parallax fraction may be too low by a factor of $\sim$2. However, in reality, the discrepancy may be less than this because on average massive stellar remnants will have larger $\tilde{r}_{\rm E}$ and correspondingly a reduced probability of exhibiting parallax signatures (see Fig. 8 and Section 4.3). In addition, since the baseline of our mock light curves is only 3 yr, events with such long time-scales may not have been considered in this analysis. For a mock event to be included in our parallax catalogue, we require a constant baseline, which excludes exceptionally long-duration events.

To date, the most promising candidate black hole event is OGLE-1999-BUL-32/MACHO-99-BLG-22 (Mao et al. 2002; Bennett et al. 2002b). This event, along with an additional two events MACHO-96-BLG-5 and MACHO-98-BLG-6 (Bennett et al. 2002a), have been analysed by Agol et al. (2002). In this paper, they used their mass estimator (see equation 14) to conclude that event OGLE-1999-BUL-32 has a probability of 76 per cent of being caused by a black hole lens (with the remaining two events having probabilities less than 20 per cent). The event parameters $t_{\rm E}$ and $\tilde{r}_{\rm E}$ for these three events can be found in Table 1. In addition to $t_{\rm E}$ and $\tilde{r}_{\rm E}$, Agol et al. (2002) also incorporated the angle of the projected velocity θ_G and the lower limit on the lens magnitude into their estimator. For events OGLE-1999-BUL-32, MACHO-96-BLG-5 and MACHO-98-BLG-6, the respective angles and I-band lens magnitude constraints are: 142°, $I_{\rm L} > 18.6$; -20°, $I_{\rm L} > 18.6$; -68°. The lower limit for the I-band lens magnitude of event MACHO-98-BLG-6 is unknown since Bennett et al. (2002a) only constrain the V-band magnitude.

Using our simulations we now attempt to determine whether the observed characteristics of these events are consistent with our stellar population (that contains no remnants). In Fig. 12, we calculate the joint probability distribution of the parameters $\tilde{r}_{\rm E}$ and $t_{\rm E}$ for the three black hole candidate events; for each event, we plot the probability distributions for the mock events that match the observed θ_G and have lens magnitudes fainter than the required limit. Note that here we do not incorporate the OGLE-II event detection efficiency, since many of these long-duration events will be omitted because of the 3-yr baseline of the experiment. From this figure, it can be concluded that although the properties of event MACHO-1998-BLG-6 are consistent with what is predicted from our simulations, the remaining two events, especially OGLE-1999-BUL-32, are clearly inconsistent. However, such large values of $\tilde{r}_{\rm E}$ can be obtained by having the lens and source close together, e.g. from bulge self-lensing. Although bulge self-lensing events typically have a shorter time-scale (with a mean $t_{\rm E}$ of 26.3 d versus 32.1 d for all events), if the Galactic model incorporated the streaming motion of the bar then it may be feasible to obtain both large $\tilde{r}_{\rm E}$ and $t_{\rm E}$ simultaneously.

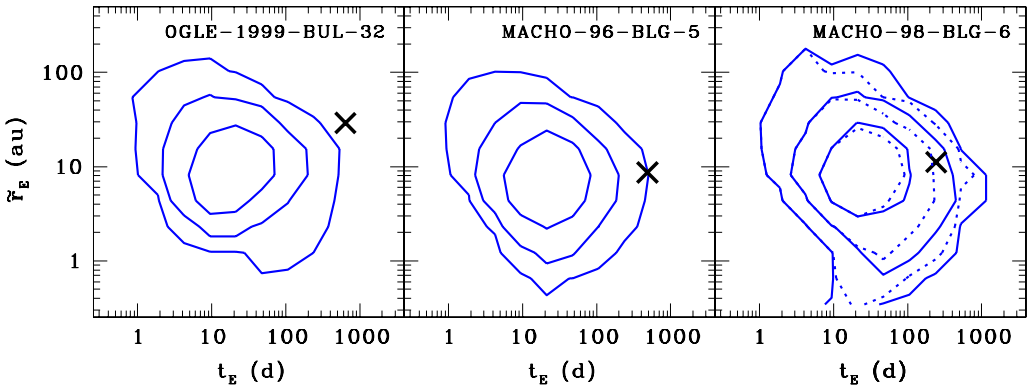

Figure 12. Contour plot showing the joint distribution of event time-scale and projected Einstein radius on the observer plane for all events regardless of whether or not they pass the OGLE-II detection criteria of Woźniak et al. (2001). The contours denote the 68.3, 95.4 and 99.7 per cent confidence regions. Each panel corresponds to the mock events that have projected velocity angle θ_G and lens magnitude consistent with the observed black hole candidate named. Note that no I-band magnitude limit is available for event MACHO-1998-BLG-6 and hence we provide two sets of contours: the solid line shows the effect of including no restriction on the lens magnitude and the dotted line corresponds to the limit $I_{\rm L} > 21.2$, which is obtained from the V-band limit $V_{\rm L} > 22.2$ (Bennett et al. 2002a) and a fiducial estimate of the colour of the lens $(V - I)_{\rm L} = 1.0$. Note that since one might naïvely suspect that $(V - I)_{\rm L} \gtrsim 1.0$, the true contours should lie somewhere between the dotted and solid contours presented here.

Downloaded from https://academic.oup.com/mnras/article-abstract/361/1/128/1021145 by University of Groningen user on 30 November 2018

5 DISCUSSION AND CONCLUSIONS

This paper has investigated the properties of parallax microlensing events towards the Galactic bulge. The expected fraction of parallax events based on standard models of the Galaxy is of the order of a few per cent, which is compatible with most observed findings. However, it should be noted that observed catalogues feature other types of exotic microlensing events, such as binary-lens events (see Jaroszyński 2002) and binary-source (xallarap) events, many of which can mimic parallax signatures and hence display an improvement in χ^2 when fit with a parallax model (e.g. Smith et al. 2002b). Although our predicted parallax fractions seem consistent with observed catalogues, there is one exception, namely the results from the EROS collaboration (Afonso et al. 2003). In this paper, they report a fraction of approximately 12.5 per cent, which is even more surprising when one considers that this catalogue is from clump-giant sources, which supposedly reside in the bulge; our simulations predict that the fraction of parallax events for bulge sources is only ∼1 per cent. It could be argued that the EROS source stars are bright red clump giant stars and as such may have higher S/N than our simulations. However, even if we restrict our simulations to bright bulge-source stars with high S/N, the percentage of events with convincing parallax signatures is only 2 per cent; given this predicted fraction, the probability that such a sample of 16 events will yield two parallax events is only 0.04. Therefore, although no strong conclusions can be drawn, it seems that this observed fraction of parallax events from the EROS catalogue may be inconsistent with our simulations.

Our models have one major shortcoming, namely that we only included blending from the lenses themselves, i.e. we did not include blending from nearby unrelated stars. We attempted to limit this problem by only considering sources brighter than $I = 19$, since it is commonly assumed that such bright sources are less affected by blending.[4] To test what effect blending from unrelated stars would have on our simulations, we perform the following simple investigation; we generate an additional catalogue of mock events with blending ratio (i.e. ratio of source flux to total baseline flux) distributed uniformly between zero and one. This means that the source stars for the blended catalogue are fainter than the corresponding source star in the unblended catalogue. Although the mean time-scale of observed events ($t_{\rm E}$) is practically unchanged in this new catalogue, the overall fraction of parallax events is slightly reduced due to the greater number of lower S/N events, which can be expected since the source stars are fainter for the blended catalogue. Currently, it is unclear how blending varies as a function of source magnitude and event time-scales, so we cannot address this question quantitatively. However, the qualitative differences between all microlensing and parallax events (i.e. the distributions shown in Section 4) appear unchanged from this analysis of blending.

To obtain a greater understanding of the underlying nature of parallax events, we examined the distributions of the event parameters $t_{\rm E}$ and $\tilde{v}$ (or, equivalently, $\tilde{r}_{\rm E}$) for parallax events, comparing them to the distributions for all events. One important question is how well do our simulations match the observed characteristics of parallax events. Although the overall fractions of parallax events seem consistent with current catalogues, we can also tentatively compare the parallax parameters such as the projected Einstein radius, $\tilde{r}_{\rm E}$. In Fig. 13, we show a plot comparing the predictions from our simulations with the distribution of $\tilde{r}_{\rm E}$ for the observed parallax events from Table 1. It should be noted that since the events from Table 1 come from a wide range of microlensing experiments with differing durations, sampling and photometric properties, any comparison can only be very speculative. However, as can be seen from the bottom panel of this figure, the observed distribution of $\tilde{r}_{\rm E}$ (as given by the data points) appears to be in reasonable agreement with the distribution from parallax events in our mock catalogues. Furthermore, from our simulations, we can calculate the efficiency of recovering parallax signatures and attempt to determine the form of the underlying $\tilde{r}_{\rm E}$ distribution for these observed events. This method is analogous to the one used to convert an observed time-scale distribution into a true underlying time-scale distribution using the 'detection efficiency'. The upper panel of Fig. 13 shows the efficiency of detecting parallax signatures, and when applied to the observed $\tilde{r}_{\rm E}$ distribution we obtain the underlying distribution shown in the middle panel. It appears that the observed distribution is consistent with the underlying $\tilde{r}_{\rm E}$ distribution from our simulations.

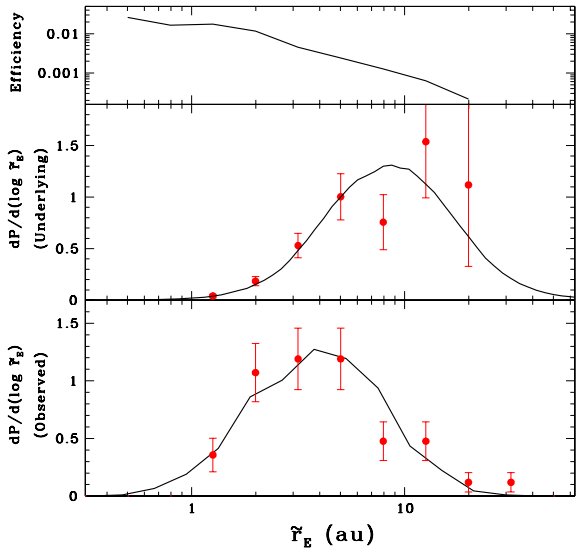

Figure 13. A comparison between the distribution of the projected Einstein radius ($\tilde{r}_{\rm E}$) for observed parallax events and our mock catalogues. The distributions from our mock catalogue are given by the solid lines and the observed distributions are given by the data points (where Poisson errors have been assumed). The lower panel shows the observed distribution, while the middle panel shows the underlying distribution, after correcting for the efficiency (top panel).

Although there are currently too few observed parallax events for us to make any firm statements about the distribution of the parallax parameters, this may change in the near future thanks to projects such as OGLE-III (Udalski 2003), which is currently detecting ∼500 microlensing events each year. Assuming the rate of parallax detection for this project is similar to that of OGLE-II, the three-fold increase in sky coverage means that a few good quality parallax events will be detected each year. It is expected that the OGLE-III project (or an upgraded experiment, OGLE-IV) will continue for many years, which should be sufficient to enable the construction of distributions of $\tilde{r}_{\rm E}$ and $\tilde{v}$ that are reasonably well-constrained. A study similar to the present one would allow a detailed comparison between theoretical predictions and observations for parallax events.

Unique lens-mass determinations for parallax events may become routine in the near future by combining a reliable measurement of $\tilde{r}_{\rm E}$ with additional constraints, such as has been shown already

[4] However, recent work by Sumi et al. (2005) has suggested that even this assumption may not be wholly reliable.

Downloaded from https://academic.oup.com/mnras/article-abstract/361/1/128/1021145 by University of Groningen user on 30 November 2018

for a number of events (An et al. 2002; Gould et al. 2004; Kubas et al. 2005). One particular approach that has been proposed is the measurement of the separation between the two microlensed images using powerful interferometers such as the Very Large Telescope Interferometer (Delplancke et al. 2001). We can see from our simulations that such image separations at maximum magnification ($\theta_{\rm sep} = \theta_{\rm E}\sqrt{u_0^2+4}$, where u_0 is the impact parameter corresponding to the maximum magnification) are larger for our parallax sample, with mean separations of 1.8 mas compared to 0.8 mas for the full sample. Therefore it will be easier to resolve the two microlensed images for parallax events and, in addition, their longer duration will make it more feasible to plan high signal-to-noise ratio observations while the events are still undergoing high magnification.

ACKNOWLEDGMENTS

MCS and VB acknowledge financial support by PPARC. MCS also acknowledges financial support from the Netherlands Organization for Scientific Research (NWO). This work has benefitted from the financial help from the visitor's grants at Jodrell Bank and Cambridge. This work was partially supported by the European Community's Sixth Framework Marie Curie Research Training Network Programme, Contract No. MRTN-CT-2004-505183 'ANGLES'. We are deeply indebted to the referee Andy Gould for providing a comprehensive and insightful report. We also wish to thank Pavel Kroupa for advice regarding the mass and luminosity functions.

REFERENCES

Afonso C. et al., 2003, A&A, 404, 145
An J. H. et al., 2002, ApJ, 572, 521
Agol E., Kamionkowski M., Koopmans L. V. E., Blandford R. D., 2002, ApJ, 576, L131
Alcock C. et al., 2000, ApJ, 541, 270
Baraffe I., Chabrier G., Allard F., Hauschildt P. H., 1998, A&A, 337, 403
Becker A., 2000, PhD thesis, Univ. of Washington
Belokurov V., Evans N. W., 2002, MNRAS, 331, 649
Bennett D. P. et al., 2002a, ApJ, 579, 639
Bennett D. P., Becker A. C., Calitz J. J., Johnson B. R., Laws C., Quinn J. L., Rhie S. H., Sutherland W., 2002b, preprint (astro-ph/0207006)
Binney J. J., Evans N. W., 2001, MNRAS, 327, L27
Bond I. et al., 2001, MNRAS, 327, 868
Buchalter A., Kamionkowski M., 1997, ApJ, 482, 782
Cseresnjes P., Alard C., 2001, A&A, 369, 778
Delplancke F., Górski K. M., Richichi A., 2001, A&A, 375, 701
Dwek E. et al., 1995, ApJ, 445, 716
Drimmel R., Spergel D. N., 2001, ApJ, 556, 181
Edvardsson B., Andersen J., Gustafsson B., Lambert D. L., Nissen P. E., Tomkin J., 1993, A&AS, 102, 603
Evans N. W. 1995, ApJ, 445, L105
Evans N. W., 2003, in Valls-Gabaud D., Kneib J.-P., eds, Gravitational Lensing: A Unique Tool For Cosmology. in press (astro-ph/0304252)
Evans N. W., Belokurov V., 2002, ApJ, 567, L119
Ghosh H. et al., 2004, ApJ, 615, 450
Gould A., 1992, ApJ, 392, 442
Gould A., 1994, ApJ, 421, L71
Gould A., 1998, ApJ, 506, 253
Gould A., 2000, ApJ, 535, 928
Gould A., 2004, ApJ, 606, 319
Gould A., Bennett D. P., Alves D. R., 2004, ApJ, 614, 404
Han C., Gould A., 1995, ApJ, 449, 521
Han C., Gould A., 2003, ApJ, 592, 172
Jahreiß H., Wielen R., 1997, ESA SP-402: Hipparcos – Venice '97, 402, 675
Jaroszyński M., 2002, Acta Astron., 52, 39
Jiang G. et al., 2005, ApJ, 617, 1307
Kubas D. et al., 2005, A&A, in press (astro-ph/0502018)
Kroupa P., 1995, ApJ, 453, 358
Kroupa P., 2002, Sci, 295, 82
Le Guillou L., 2003, PhD thesis, CEA/Saclay
Mao S., Paczyński B., 1996, ApJ, 473, 57
Mao S., Paczyński B., 2002, MNRAS, 337, 895
Mao S. et al., 2002, MNRAS, 329, 349
Paczyński B., 1986, ApJ, 304, 1
Paczyński B., 1996, ARA&A, 34, 419
Paczyński B., 1998, ApJ, 494, L23
Park B.-G. et al., 2004, ApJ, 609, 166
Paulin-Henriksson S. et al., 2003, A&A, 405, 15
Popowski P., 2001, MNRAS, 321, 502
Popowski P. et al., 2004, ApJ submitted (astro-ph/0410319)
Soszyński I. et al., 2001, ApJ, 552, 731
Smith M. C., 2003, MNRAS, 343, 1172
Smith M. C. et al., 2002a, MNRAS, 336, 670
Smith M. C., Mao S., Woźniak P., 2002b, MNRAS, 332, 962
Smith M. C., Mao S., Woźniak P., 2003a, ApJ, 585, L65
Smith M. C., Mao S., Paczyński B., 2003b, MNRAS, 339, 925
Stanek K. Z., 1995, ApJ, 441, L29
Stanek K. Z., 1996, ApJ, 460, L37
Stanek K. Z., Udalski A., Szymański M., Kałużny J., Kubiak M., Mateo M., Krzemiński W., 1997, ApJ, 477, 163
Sumi T. et al., 2003, ApJ, 591, 204
Sumi T. et al., 2005, ApJ submitted (astro-ph/0502363)
Udalski A., 2003, Acta Astron., 53, 291
Walker M. A., 1995, ApJ, 453, 37
Witt H. J., Mao S., 1994, ApJ, 430, 505
Woźniak P. R., 2000, Acta Astron., 50, 421
Woźniak P. R., Udalski A., Szymański M., Kubiak M., Pietrzyński G., Soszyński I., Żebruń K., 2001, Acta Astron., 51, 175
Woźniak P. R., Udalski A., Szymański M., Kubiak M., Pietrzyński G., Soszyński I., Żebruń K., 2002, Acta Astron., 52, 129
Zheng Z., Flynn C., Gould A., Bahcall J. N., Salim S., 2001, ApJ, 555, 393
Zoccali M., Cassisi S., Frogel J. A., Gould A., Ortolani S., Renzini A., Rich R. M., Stephens A. W., 2000, ApJ, 530, 418

This paper has been typeset from a TEX/LATEX file prepared by the author.

Downloaded from https://academic.oup.com/mnras/article-abstract/361/1/128/1021145 by University of Groningen user on 30 November 2018